White Rose Research Online

eprints@whiterose.ac.uk
https://eprints.whiterose.ac.uk
Universities of Leeds, Sheffield and York

Deposited via The University of York.

White Rose Research Online URL for this paper:
https://eprints.whiterose.ac.uk/id/eprint/222277/

Version: Published Version

Article:
Maharjan, Asim, Waiba, Prashant, Shrestha, Shreya et al. (2024) When a lensless fluorometer outperforms a lensed system. Optica. pp. 1124-1128. ISSN: 2334-2536

https://doi.org/10.1364/OPTICA.527289

Reuse
This article is distributed under the terms of the Creative Commons Attribution (CC BY) licence. This licence allows you to distribute, remix, tweak, and build upon the work, even commercially, as long as you credit the authors for the original work. More information and the full terms of the licence here:
https://creativecommons.org/licenses/

Takedown
If you consider content in White Rose Research Online to be in breach of UK law, please notify us by emailing eprints@whiterose.ac.uk including the URL of the record and the reason for the withdrawal request.

UNIVERSITY OF LEEDS
University of Sheffield
UNIVERSITY of York

OPTICA

When a lensless fluorometer outperforms a lensed system

Asim Maharjan,[1,†] Prashant Waiba,[1,†] Shreya Shrestha,[1,†] Rijan Maharjan,[1] Augusto Martins,[2] Kezheng Li,[2] Emiliano R. Martins,[3] Thomas F. Krauss,[2] and Ashim Dhakal[1,*]

[1]Biophotonics Lab, Phutung Research Institute, Tarakeshwar-7, Kathmandu, 44611, Nepal
[2]School of Physics, Engineering and Technology, University of York, New York, YO10 5DD, UK
[3]Department of Electrical & Computer Engineering, University of São Paulo, São Paulo 13566-590, Brazil
[†]These authors contributed equally to this work.
*ashim.dhakal@phutung.org.np

Received 16 April 2024; revised 25 June 2024; accepted 25 June 2024; published 8 August 2024

The excitation and collection of optical signals using lenses form the basis for many applications in imaging, nephelometry, fluorometry, and spectroscopy. While lenses are needed for imaging systems, their use is not so obvious for volume sensing applications. Here, we study the excitation and collection of fluorescence signals to show that lensless systems generally provide a stronger signal compared to lensed systems for the case of extended Lambertian-like sources, such as LEDs. To elucidate this result, we provide a foundational framework to analyze the signal collection efficiency from an arbitrary detection volume with and without lenses when extended sources and detectors are used. A combination of factors, including the limited numerical aperture, the use of extended sources/detectors, and the requirement of a finite imaging distance between the source/detector, lenses, and the sample, limits the performance of the lensed system compared to the lensless system. Our theoretical and experimental results indicate that conventional wisdom based on the assumption of point-like sources and detectors should not always be followed. We provide a systematic approach for analyzing and simplifying the design of low-cost, lensless fluorometers and nephelometers without sacrificing their performance, reporting a sub-ppb level detection limit for measuring tryptophan-like-fluorescence in drinking water.

Published by Optica Publishing Group under the terms of the Creative Commons Attribution 4.0 License. Further distribution of this work must maintain attribution to the author(s) and the published article's title, journal citation, and DOI.

https://doi.org/10.1364/OPTICA.527289

1. INTRODUCTION

Optical methods, such as fluorescence spectroscopy, fluorimetry, and nephelometry, are emerging as new sensing paradigms for assessing microbial contamination in drinking and environmental water [1–3]. Such optical methods have been shown [4] to be more rapid and robust than the traditional approach of plate counting of indicator organisms, which can take 12–48 h to produce results and requires trained personnel. Additionally, the optical techniques are inherently reagentless, which reduces cost and complexity, eliminating a specialized supply chain for the reagents, thereby simplifying implementation in resource-limited settings. The instrumentation often uses LEDs as the excitation source and measures the optical signal using an optical filter and a photodiode (PD). Due to the availability of efficient and low-cost components, these systems can be made practical as well as cost-effective.

Current fluorometers or nephelometers typically use a pair of lenses to collimate and focus the excitation light onto the target sensing volume, such as a water sample in a cuvette. The corresponding optical signal (e.g., fluorescence or scattered light) is then collected and focused onto the detector using lenses (see Fig. 1). Use of lenses has a number of advantages, such as collimation for typical dichroic filters, or localizing sample volume when specific sample regions are of interest. However, excitation and collection for a lens depends on the numerical aperture (NA) of the lenses. For simplicity, we assume that all the lenses have the same NA, then the overall dependence on the efficiency of excitation and collection of the signal scales with NA^4 [see Eq. (3)]. This strong dependence on NA implies that lenses with high NA and high transmission are required for high-efficiency systems. High-NA lensed systems also require precise optical alignment. These are challenging requirements in terms of cost and complexity, particularly for fluorometers operating in the UV regime required for the microbiological assessment of drinking water. We exemplify these challenges with a fluorometer that measures tryptophan-like fluorescence (TLF) [3], with the excitation centered around 280 nm and the fluorescence centered around 340 nm.

In addressing these challenges, two important aspects need to be considered. First, since we utilize the fluorometer to measure concentration of tryptophan in aqueous solution as an exemplar, the total optical power is the quantity of interest, for which imaging optics are not essential. Second, in line with the low cost

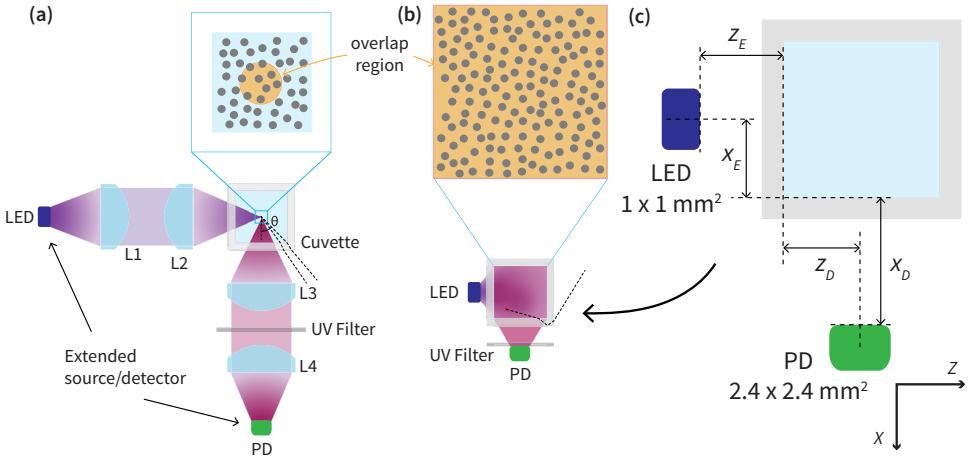

Fig. 1. (a) Schematic of a lensed setup typically used in a fluorometric or nephelometric system. The system operates with extended source and detector; (b) schematic of a lensless setup, highlighting the large excitation and collection (measurement) volume encompassing the field of view of both of the source and detector. The dots in both images represent fluorescent or scattering particles; black dashed lines represent light rays (some of which undergo total internal reflection) that do not contribute to the signal in our analysis, as they exit at an angle $\theta >$ acceptance angle ($\sim$24° for lensed, $\sim$27° for lensless system in our experiments). (c) Details in (b) showing positional variables used in this paper.

requirement, we use an LED for the 280 nm excitation and a silicon PD for the detection; both source and detector extend over a finite area. These characteristics suggest that one should apply the principles of non-imaging optics [5,6] to this problem. We note that most of the literature on non-imaging systems is centered on applications such as solar concentrators [7], displays [8], and computer graphics [9,10], while fluorometric or nephelometric applications are rarely considered. Therefore, we first develop a theoretical framework for studying the efficiency of a fluorometer with an extended source and detector, then compare the conventional lensed approach with a lensless approach. Informed by this model, we then provide experimental evidence that the lensless approach outperforms the lensed approach when considering practical limitations. This result has the added benefit of simplicity and robustness, all of which are essential for translation into a high-performance system that can be used in a resource-limited setting.

2. THEORETICAL MODEL

To avoid confusion due to different notations and definitions used in the literature, we use radiometric terminologies and symbols based on ISO standard 9288:2022 on Heat Transfer by Radiation [11] (please see Supplement 1, Table I for a list of radiometric quantities used in this paper). We model the excitation source as a collection of infinitesimal Lambertian emitters with a constant radiosity (or, radiant exitance) J_0, such that the irradiance at an arbitrary point $\vec{r}$ in the sample space is given by the radiator view-factor $F_R(\vec{r})$, which provides the sum of contributions from all of the elements on the emitter surface to that point (see Supplement 1, Section 1). View-factor is closely related to the acceptance angle of an optical system or the solid angle subtended by the optical rays, with a relationship $\Omega_R = \pi F_R(\vec{r})$ for a Lambertian radiator in a free-space. Similarly, we model the detector as a collection of infinitesimal Lambertian detection elements to determine the detector view-factor $F_D(\vec{r})$, which is the sum of the optical powers detected by each detection element from an arbitrary emitting volume element with unit radiant intensity in the sample space (see Supplement 1, Section 2). We then define the effective volume V_{eff} as the overlap integral between the two view-factors in the sample volume. The V_{eff} describes the collected power and is therefore the figure of merit of the system.

To describe the fluorescence signal, we consider isotropically absorbing and emitting fluorophores that are uniformly distributed in the sufficiently large sample space with number density ρ and fluorescence cross-section σ [12]. In what follows we will only consider the linear scattering and fluorescence process and ignore any non-linear effects. The signal power Φ_D detected by the detector is then given by (see Supplement 1, Section 3)

$$\Phi_D = \frac{1}{6} J_0 \rho \sigma V_{\text{eff}}, \tag{1}$$

where the effective volume V_{eff} is given by the integral of the view-factor overlap defined as $F_{\text{RD}}(\vec{r}) = F_R(\vec{r}) F_D(\vec{r})$ over the whole sample or cuvette volume V_{cuv}:

$$V_{\text{eff}} = \int_{V_{\text{cuv}}} F_{\text{RD}}(\vec{r}) \mathrm{d}V(\vec{r}). \tag{2}$$

Similarly, for lensed setups the view-factor overlap $F'_{\text{RD}}(\vec{r})$ calculated for the images $F'_R(\vec{r})$ and $F'_D(\vec{r})$ of the source and the detector in the sample volume provides the effective volume (see Supplement 1, Section 4):

$$V'_{\text{eff}} = (\text{NA}_{W,R})^2 (\text{NA}_{W,D})^2 \int_{V_{\text{cuv}}} F'_{\text{RD}}(\vec{r}) \mathrm{d}V(\vec{r}). \tag{3}$$

Here, $\text{NA}_{W,R}$ and $\text{NA}_{W,D}$ are the "working numerical aperture" of the imaging system used respectively at the radiator and detector sides. The working numerical aperture NA_W accounts for the distances between the lens, the object, and image to achieve a magnification m with a lens of an object-side numerical aperture NA, and is given by (see Supplement 1, Section 4 for details; see also [13,14])

$$\text{NA}_W = \frac{\text{NA}}{\sqrt{\text{NA}^2 + (1+m)^2 (1 - \text{NA}^2)}} \approx \frac{\text{NA}}{1+m}. \tag{4}$$

The approximation in Eq. (4) is valid for NA $\ll 1$. Since we wish to compare the detected optical power for two systems using identical excitation sources, detectors, and samples, the following ratio between their effective volumes corrected by the transmission τ_F of the optical filters and transmission τ_L of the lenses used is the quantity of interest:

$$\Gamma = \frac{\tau_F}{\tau_F' \tau_L} \frac{V_{\text{eff}}}{V_{\text{eff}}'}. \tag{5}$$

For both lensed and lensless systems, we are comparing the excitation using the same source, emission from the same material with the same optical properties, and using the same cuvette. Therefore, we neglect the dependence of the effective volumes on refractive indices of the cuvette and the liquid, excitation wavelength, or emission wavelengths. Similarly, we will not consider total internal reflection (TIR) at the cuvette-air interface and the cuvette-water interface, because in most practical scenarios the critical angle for TIR is larger than the acceptance angle of the optics [as is the case in our experiments; see also Fig. 1 and Supplement 1, Section 3, Fig. S6(a)].

3. THEORETICAL RESULTS

Let us consider the two representative setups illustrated in Fig. 1, namely, the lensed setup and the lensless setup, with an LED emitter of area 1 mm × 1 mm, a PD of area of 2.4 mm × 2.4 mm, and a sufficiently thin cuvette with size 10 mm × 10 mm × 40 mm. These dimensions are realistic and consistent with the sizes used in our experiments and in typical setups. Further, for simplicity, in this first study, we neglect transmission losses (i.e., $\tau_F = \tau_F' = \tau_L = 1$), obscuration, and aberrations. We assume that the LED and PD are placed at the center of the cuvette wall (i.e., $x_D = z_E = 0$ and $z_D = x_E = 5$ mm; air gap is assumed to be negligible).

Figures 2(a) and 2(b) show the corresponding view-factor overlap $F_{\text{RD}}(\vec{r})$ profiles calculated numerically for lensless and lensed ($m = 1$, NA $= 1$) systems, respectively. We note that $F_{\text{RD}}(\vec{r})$ for the lensless setup is distributed over a larger volume with lesser magnitude while $F_{\text{RD}}'(\vec{r})$ for the lensed system is concentrated in a small sample volume with higher magnitude near the center of the cuvette. This trade-off between the measurement volume and the $F_{\text{RD}}(\vec{r})$ magnitude is a consequence of two facts. First, for optical systems with negligible loss, the etendue G_R is conserved [15], i.e., $G_R = A_R \Omega_R = A_R(\pi F_{R\to S}') \approx A_S \Omega_S$, such that when the light is concentrated in a smaller area A_S, it must diverge to a larger solid angle Ω_S losing its radiant intensity outside the small volume near A_S. Second, unlike the lensless system where the LED and PD are physically separated by a finite distance, in the lensed system they can be imaged at the center of the cuvette to obtain enhanced overlap with the required magnification by design. For the ideal condition (i.e., NA $= 1$, $m = 1$), the V_{eff} ratio is $\Gamma = 0.13$ for a lensed system, providing about 7.7 times more signal than a lensless system.

We now consider more practical scenarios, starting with the numerical aperture. Here, we note that the benefits of small measurement volume and high view-factor overlap for a lensed system quickly diminish as the NA of the lenses is reduced, due to the fourth-power dependence on NA. This can be seen in Fig. 2(c), where the $F_{\text{RD}}'(\vec{r})$ is plotted for a more practical lens of NA $= 0.4$, providing $\Gamma = 61.7$ times more signal for lensless systems than for lensed systems. More generally, as shown in Fig. 2(d), for the LED, PD, and cuvette sizes considered here, a lensed system provides a higher signal than a lensless system only for NA > 0.83. If, in addition, we consider the distance between the cuvette and the LED or PD, which typically has to be greater than zero for practical reasons, we note that the boundary shifts to slightly lower NA.

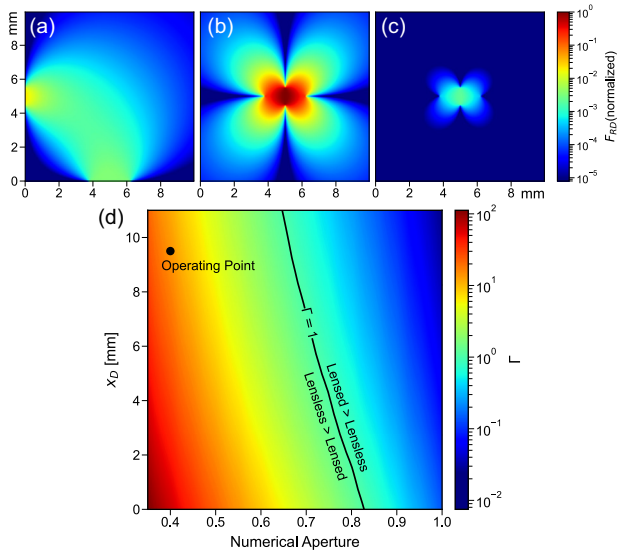

Fig. 2. Distribution of the view-factor overlap $F_{\text{RD}}(\vec{r})$ for: (a) the lensless configuration where the LED and the PD are placed next to the cuvette wall ($z_E = x_D = 0$) at the center ($x_E = z_D = 5$ mm); (b) ideal lensed setup with NA $= \tau_L = \tau_F = m = 1$ for both excitation and collection sides; (c) lensed setup under realistic conditions with NA $= 0.4$, $m = 1$ demonstrating significant reduction in the overlap; (d) effect of the NA of the lenses and the photodiode distance (x_D) from the cuvette wall on the ratio Γ between the effective volumes for lensed and lensless systems. The black line corresponds to the values where the lensed and lensless systems perform equally. To the left of this line, the lensless system performs better than the lensed system. We also include the operating point of our system, with all parameters described in Section 4, where the efficiency ratio between the two systems is $\Gamma = 13.5$.

4. EXPERIMENTAL RESULTS

To put our model into a practical context, we first measure the emission profile of the LED (see Supplement 1, Section 6) used in our experiments. For the plano-convex lenses used in our experiments (NA $= 0.38 \pm 0.02$, $m = 1 \pm 0.01$, $\tau_L = 0.81$), we also account for the obscuration due to finite lens size, cuvette walls, and the transmission of the optical elements. Correspondingly, for the lensless system, we account for the transmission of the bandpass filter ($\tau_F = 0.38$) and the distances of the LED/PD from the cuvette (summarized in Fig. S4 in Supplement 1, Section 6), which are the limiting factors for the signal collection. Using these experimentally determined values, we numerically evaluate $F_{\text{RD}}(\vec{r})$ and $F_{\text{RD}}'(\vec{r})$ shown in Figs. 3(a) and 3(b) and numerically determine the ratio between the lensless and the lensed system Γ_{num} to be $\Gamma_{\text{num}} = 2.07 \pm 0.38$; so we predict that the lensless system is superior by a factor of $\sim$2.1.

Next, we compare the two systems experimentally by measuring the fluorescence signal obtained from aqueous tryptophan (Trp) solutions of various concentrations. The results are shown in Fig. 3(c), where we consistently observe a ratio $\Gamma_{\text{exp}} = 2.0 \pm 0.2$ between the two systems, for a wide concentration range between

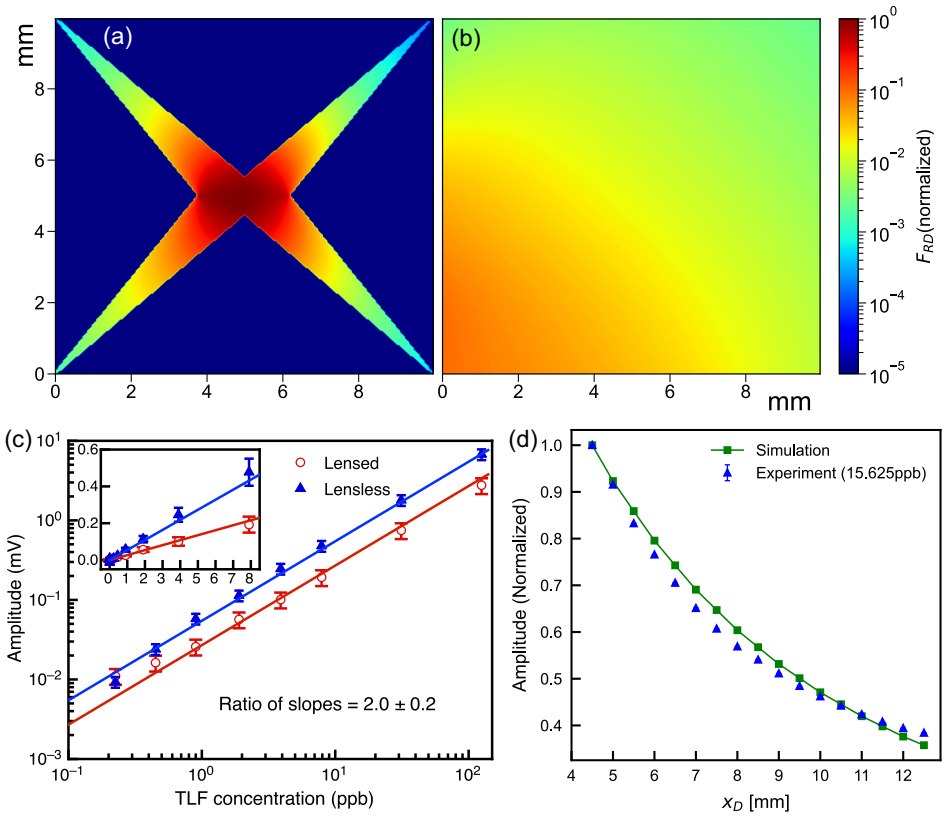

Fig. 3. Distribution of the view-factor overlap $F'_{\mathrm{RD}}(\vec{r})$ for experimental cases: (a) lensed system with NA $= 0.38 \pm 0.02$, $m = 1 \pm 0.01$, $\tau_L = 0.81$; accounting for the obscuration due to the cuvette wall and the lens tube leads to shadowing of the conical section near the wall (see Supplement 1, Fig. S5); (b) lensless system with filter transmission $\tau_F = 0.38$, $x_E = 2$ mm, $z_E = 4.3$ mm, $x_D = 9.5$ mm, and $z_D = 4$ mm [refer to Fig. 1(c) for the parameters; see also Supplement 1, Fig. S4]. Effective volumes and transmissions shown in (a) and (b) numerically provide the signal ratio $\Gamma_{\mathrm{num}} = 2.07 \pm 0.38$. (c) The fluorescence intensity ratios from Trp solution as a function of concentration as measured by the lensless and lensed systems, providing $\Gamma_{\mathrm{exp}} = 2.0 \pm 0.2$ in very good agreement with the numerical calculations. Error bars represent input errors in the fitting algorithm to obtain reduced-$\chi^2 \approx 1$; (d) variation of fluorescence signal amplitude (normalized to maxima, for 15.625 ppb concentration of Trp in the cuvette) as the distance between the cuvette and detector x_D is varied while $x_E = 4$ mm, $z_E = 1.3$ mm, $z_D = 6.5$ mm are kept fixed [please refer to Fig. 1(c) for the parameters; see also Supplement 1, Fig. S4].

1 ppb and 100 ppb, agreeing with our numerical evaluation within the experimental error.

To further verify our theoretical model, we measured the collected Trp fluorescence signal as a function of the distance x_D of the PD from the cuvette (see Fig. S4, Supplement 1, Section 6 for complete geometry). Other distances and the concentration were kept fixed. The comparison of the experimental results with the normalized values of V_{eff} calculated numerically using our model [Eq. (2)] again demonstrates good agreement between experiments and the proposed model [Fig. 3(c)]. A similar relationship between z_E and signal is expected due to a similar (inverse-square) relationship with the distance for both radiator and detector view-factors [see Eq. (S6) and Eq. (S12)].

5. DISCUSSION

The key result we report here is that a lensless fluorometer generally outperforms a lensed system when practical boundary conditions are considered. The reason for this result is the trade-off between the measurement volume and optical power concentration as a consequence of the conservation of etendue, which in an optical system is characterized by the inverse relationship between the divergence of the radiation or acceptance angles (which are directly related to the view-factor) and the area of the source. Lensless systems, using large-area sources and detectors, typically exhibit smaller divergence, but they may operate over a large measurement volume. Conversely, a lensed system of sufficiently large NA may exhibit a large acceptance angle but only in a small detection volume. As a consequence of this trade-off, a lensless system collects nearly as much power as an *ideal* lensed system, and more optical power than a *practical* lensed system. This trade-off is not apparent when the sources are assumed to be a point-source (where the entendue is almost zero), as is assumed in many scenarios for simplicity. In fact, larger LED/PD sizes provide an even higher signal for lensless systems (see Supplement 1, Fig. S8).

Please note that unity magnification, as considered here, represents the best case scenario for the lensed system. A magnification $m > 1$ for a fixed object distance and NA requires longer image distance, thereby reducing the working NA as per Eq. (4). Similarly, a magnification $m < 1$, for a fixed image distance requires a longer object distance, which reduces the NA of the effective lens system and the measurement volume (see Supplement 1, Fig. S8).

A lensed system becomes necessary when a small sensing volume is desired, or when a very small source/detector is used, or when collimated light such as from a laser needs to be focused to as small an area as possible. Note that even in the case of laser illumination, the lenses need to have an NA of $0.7 - 0.8$ to break

even, which is much higher than the NAs used in most practical fluorometer instruments. Smaller detectors are sometimes also preferred for their lower noise-equivalent power (NEP). In Supplement 1, Section 8 we provide experimental results with dilution experiments for a smaller PD of area 1.1 mm × 1.1 mm and NEP = 6.8×10^{-16} W/$\sqrt{\text{Hz}}$ and compare it with the PD of area 2.4 mm × 2.4 mm and NEP = 2.5×10^{-15} W/$\sqrt{\text{Hz}}$. We observe that the signal collection efficiency is approximately proportional to the increase in the area of the PD, and that the detection limit is given by the signal collection efficiency, not the NEP, so there is no obvious penalty for using a larger photodiode.

Lensless systems are limited by the cuvette size, LED/PD sizes, and the distance between the LED/PD with the cuvette. Due to the inverse-square relationship of the view-factors with the distances, one expects a higher overlap if the source and detector are placed near to one another (see Supplement 1, Fig. S9c). However, the geometry is limited by practical considerations such as cuvette size, thermal and optical cross-talk (due to possible direct optical paths) between the LED and the detector, and the space required for optical filters. Additionally, the sensing volume for a lensless system can also be limited due to the inner-filter effects (e.g., strong absorption by the fluorophores, which for lensed systems can be managed by imaging a smaller volume near the surface). A hybrid configuration, e.g., where lenses are used for the LED source and no lenses are used for the detector, presents a compromise, which is illustrated in Supplement 1, Section 9 for the interested readers. Lensed systems are limited by their NA, obscurations, aberrations, and other losses. In addition to requiring a near-perfect lens, a lensed system of higher NA also requires more precise alignment (see Supplement 1, Section 7), losing ∼30% of light for a misalignment of 1 mm. Lensless systems lose ∼5% for same misalignment. Consequently, apart from higher performance for practical parameters, the lensless system may be made more compact and robust and may be realized with lower-cost components and manufacturing tolerances.

To conclude, we have introduced and experimentally verified a theoretical framework to study and optimize the efficiency of excitation and collection of optical power from a sample volume for non-imaging sensing applications, such as fluorometers or nephelometers. Our numerical and experimental results demonstrate that a lensless fluorometer/nephelometer generally outperforms a realistic lensed system. Moreover, we demonstrated a lensless fluorometer that can achieve the level of sensitivity required (<1 ppb) for detecting fecal contamination in drinking water as stipulated by the WHO; this important result paves the way for realizing a low-cost, high-performance system for drinking water assessment in a resource-limited setting.

Funding. Optica Foundation (20th Anniversary Challenge 2022); Engineering and Physical Sciences Research Council (EP/P030017/1,EP/T020008/1, EP/W524165/1); The World Academy of Sciences (18-013 RG/PHYS/AS_I, 21-334 RG/PHYS/AS_G, 22-244 RG/PHYS/AS_G); Fundação de Amparo à Pesquisa do Estado de São Paulo (2020/00619-4, 2021/06121-0); Conselho Nacional de Desenvolvimento Científico e Tecnológico (307602/2021-4).

Acknowledgment. A.D. acknowledges the Optica Foundation's 20th Anniversary Challenge Prize 2022. R.M. acknowledges QuantumSoft for providing Pro Fit software.

Disclosures. The authors declare no conflicts of interest.

Data availability. Data underlying the results presented in this paper are not publicly available at this time but may be obtained from the authors upon reasonable request.

Supplemental document. See Supplement 1 for supporting content.

REFERENCES

1. S. J. Hart and R. D. JiJi, "Light emitting diode excitation emission matrix fluorescence spectroscopy," Analyst **127**, 1693–1699 (2002).
2. J. Bridgeman, A. Baker, D. Brown, *et al.*, "Portable LED fluorescence instrumentation for the rapid assessment of potable water quality," Sci. Total Environ. **524-525**, 338–346 (2015).
3. S. Cumberland, J. Bridgeman, A. Baker, *et al.*, "Fluorescence spectroscopy as a tool for determining microbial quality in potable water applications," Environ. Technol. **33**, 687–693 (2011).
4. J. P. Sorensen, J. Nayebare, A. F. Carr, *et al.*, "In-situ fluorescence spectroscopy is a more rapid and resilient indicator of faecal contamination risk in drinking water than faecal indicator organisms," Water Res. **206**, 117734 (2021).
5. J. Chaves, *Introduction to Nonimaging Optics* (CRC Press, 2017).
6. R. Winston, L. Jiang, and M. Ricketts, "Nonimaging optics: a tutorial," Adv. Opt. Photon. **10**, 484–511 (2018).
7. N. Jost, T. Gu, J. Hu, *et al.*, "Integrated microscale concentrating photovoltaics: a scalable path toward high-efficiency, low-cost solar power," Solar RRL **7**, 2300363 (2023).
8. I. Moreno, M. Avendaño-Alejo, and C. P. Castañeda-Almanza, "Nonimaging metaoptics," Opt. Lett. **45**, 2744–2747 (2020).
9. C. M. Goral, K. E. Torrance, D. P. Greenberg, *et al.*, "Modeling the interaction of light between diffuse surfaces," ACM SIGGRAPH Comput. Graph. **18**, 213–222 (1984).
10. J. R. Wallace, K. A. Elmquist, and E. A. Haines, "A ray tracing algorithm for progressive radiosity," in *16th Annual Conference on Computer Graphics and Interactive Techniques*, ACM, New York, New York, USA, 1989.
11. Organization for Standardization, "Thermal insulation, heat transfer by radiation, vocabulary (ISO 9288:2022)," (Organization for Standardization, 2022).
12. R. Carminati and J. C. Schotland, *Principles of Scattering and Transport of Light* (Cambridge University, 2021).
13. M. Born, E. Wolf, and A. B. Bhatia, *Principles of Optics: Electromagnetic Theory of Propagation, Interference and Diffraction of Light*, 7th ed. (Cambridge University, 1999).
14. J. M. Palmer and B. G. Grant, *The Art of Radiometry* (SPIE, 2010).
15. International Commission on Illumination, 17-21-048, [accessed 2024-02-08], https://cie.co.at/.

144.32.225.234 (b) 2025-01-23 11:30:45